



Universiteit
Leiden
The Netherlands

Hot chemistry and physics in the planet-forming zones of disks

Bast, J.E.

Citation

Bast, J. E. (2013, January 10). *Hot chemistry and physics in the planet-forming zones of disks*. Retrieved from <https://hdl.handle.net/1887/20396>

Version: Corrected Publisher's Version

License: [Licence agreement concerning inclusion of doctoral thesis in the Institutional Repository of the University of Leiden](#)

Downloaded from: <https://hdl.handle.net/1887/20396>

Note: To cite this publication please use the final published version (if applicable).

Cover Page



Universiteit Leiden



The handle <http://hdl.handle.net/1887/20396> holds various files of this Leiden University dissertation.

Author: Bast, Jeanette Elisabeth

Title: Hot chemistry and physics in the planet-forming zones of disks

Issue Date: 2013-01-10

IV

Investigation of HCN excitation in protoplanetary disks¹

Context HCN absorption and emission vibration-rotation lines originating from inner planet-forming zones of protoplanetary disks have so far been modeled using local thermodynamical equilibrium (LTE) slab and disk models. However, it has not yet been investigated whether LTE is a good approximation for these HCN emitting regions.

Aim This study investigates how the HCN excitation at 3 and 14 μm is impacted by non-LTE conditions and radiative pumping.

Methods Observed line fluxes at 3 and 14 μm are compared with modeled line fluxes by using a radiative transfer slab and disk model assuming LTE. These line fluxes are then compared to the modeled line fluxes using a non-LTE slab model with different excitation temperatures, volume densities and column densities of HCN. An infrared radiation field is also included to see how the line fluxes are impacted by radiative pumping.

Results The 3 μm line flux reaches LTE at a much higher density of around 10^{14} cm^{-3} relative to the 14 μm line fluxes which reaches LTE at around 10^9 cm^{-3} . This means that the 3 μm line fluxes are much less well modeled by assuming LTE. In addition it is shown that radiative pumping can significantly impact the line fluxes, especially of the 3 μm lines. The observed 3 μm /14 μm flux ratio cannot be modeled by a LTE slab model unless the volume density is $10^{13} - 10^{14} \text{ cm}^{-3}$ at a temperature of $\sim 900 \text{ K}$ which is at least 1 to 2 magnitudes higher than the expected volume density in the region from which this emission is assumed to originate. However, the observed flux ratio can be modeled when including non-LTE and radiative pumping using densities as low as 10^9 cm^{-3} at a temperature

¹J.E. Bast, S. Bruderer, D. Harsono, B. Brandl, A.G.G.M. Tielens and E. F. van Dishoeck

of 900 – 1200 K.

Conclusions Both LTE slab and disk models overestimate the 3 μm and to some extent the 14 μm HCN line fluxes and hence underestimate the HCN abundance. The conclusion can therefore be made that non-LTE conditions and radiative pumping are important to implement in future protoplanetary disk models.

4.1 Introduction

The first million years of a low mass star’s life is an exciting period since this is the time when the gas and dust, mainly in the inner part (< 10 AU) of the disk around the star, transforms into building blocks for new planets. It is important to determine the chemical composition and evolution of the gas in these parts of the circumstellar disks since they provide the initial conditions for the type of atmospheres, surfaces and structures that these planets will consist of. One way to extract information about the chemistry in these disks is to observe which molecules are present and determine their relative abundances. In addition information about the physical conditions such as the temperature, which type of radiation dominates in different regions, the density of the gas and the ratio between the gas and dust will decide the chemical evolution of the gas in the disks. Several studies have been done of different molecules by detecting their emission lines in the planet-forming regions of disks, such as CO (e.g., Najita et al. 2003, Brittain et al. 2003, 2007, 2009, Blake & Boogert 2004, Pontoppidan et al. 2008, Salyk et al. 2011b, Brown et al. *subm.*); OH, H₂O (Carr et al. 2004, Carr & Najita 2008, Mandell et al. 2008, Salyk et al. 2008, Najita et al. 2010, Pontoppidan et al. 2010, Salyk et al. 2011, Carr & Najita 2011, Fedele et al. 2011); and HCN, C₂H₂, and CO₂ (Carr & Najita 2008, 2011, Najita et al. 2010, Salyk et al. 2011, Mandell et al. 2012). In some cases also absorption in edge-on disks has been used to detect HCN, C₂H₂, and CO₂ (Lahuis et al. 2006, Gibb et al. 2007, Doppmann et al. 2008, Kruger et al. 2011, Bast et al. *subm.*).

These studies use observations of molecular lines to infer the abundance structure of the molecule of interest by adopting either a slab or disk model. By modelling the lines also physical conditions such as the temperature of the emitting gas can be estimated. However these models mainly use local thermodynamical equilibrium (LTE) as an approximation to model the lines. This means that a single temperature sets the population of the excitation levels of the molecule by using the Boltzmann equation and that by implication the density is very high in order to thermalize the levels. This assumption is used since including non-LTE processes, especially in radiative transfer disk models, is complicated. In addition in many cases collisional rate coefficients for the specific molecule of interest have yet not been measured or calculated which are needed to model the lines under non-LTE conditions. The inner regions of protoplanetary disks have so far been assumed to have such high temperatures and densities so that LTE is a good approximation. However a recent study of water emission lines originating from

within 0.2 AU of the disk done by Meijerink et al. (2009) shows that using LTE in a disk model can introduce large errors in both the H₂O abundance and temperature structure of the emitting gas. That LTE is not a good approximation can be explained by the fact that the main part of the IR emission from the water lines arises in the surface of the disk where the densities are too low to provide the conditions needed for LTE. The errors in the estimated water abundance will also impact the entire view of the chemistry and chemical evolution of the disks. Since water is such an important molecule in the reaction network to form many other molecules in the disk, it is very important to have a correct determination of its abundance.

HCN is another important reactant in the chemical network of these disks (Agúndez et al. 2008, Walsh et al. 2012). Besides its role in the chemistry, HCN has another valuable characteristic, namely a dipole moment. The dipole moment means that it can be observed both at infrared wavelengths, through its ro-vibrational transitions, and at millimeter wavelengths, through its pure rotational transitions. This means that HCN is one of the few molecules that simultaneously can probe both the inner and outer parts of the disk and therefore can help to understand how the chemical structure of the disk changes with radius.

Observations of HCN suggest that the infrared emission from this molecule has a very similar origin as the water infrared emission (Salyk et al. 2011, Mandell et al. 2012). Salyk et al. (2011) used a LTE slab model to model the HCN Q-branch lines of the unresolved ν_2 mode at 14 μm observed using *Spitzer*. Mandell et al. (2012) modeled their observed HCN ν_3 mode emission lines at 3 μm by using both a LTE slab model and a radiative transfer disk model assuming LTE in each grid point of the disk. It was shown that the inferred abundance ratios of HCN relative to other observed molecules did not differ much between the two methods, probably because the errors introduced by the LTE assumption are comparable for the various species. However, the absolute abundances depend much more sensitively on the adopted method. HCN has also been detected through absorption lines in two sources at 14 μm by Lahuis et al. (2006) and Bast et al. (subm.) and one source at 3 μm by Gibb et al. (2007) and Doppmann et al. (2008) using a LTE absorption slab model. Again, only abundances relative to other molecules have been derived. Neither the emission nor the absorption observations of HCN have ever been modeled using a non-LTE slab or disk model.

Since describing the water emission using a non-LTE disk model has been proven to be a better approach than assuming LTE a similar investigation is performed here for HCN. As a first step, we investigate here the non-LTE effects on the 3 and 14 μm lines by comparing a LTE and non-LTE slab model rather than a full disk model. This will allow us to obtain insight into how non-LTE excitation impacts the line fluxes and whether this translates into different conclusions between line emission at 3 and 14 micron. A disk model is used to determine the typical temperatures and densities in the regions from which the 3 and 14 μm lines originate and to provide a reference for comparison with LTE excitation. In addition the impact of an infrared radiation field inducing radiative pumping is studied to see

which type of excitation processes of HCN are important in these regions. These results will decide if non-LTE and radiative pumping effects are important to include in the development of future radiative transfer models of protoplanetary disks (Bruderer et al., in prep.) and therefore also in the determination of the HCN abundance structure in the disks.

The different vibrational modes of the HCN molecule and the observations of HCN emission at 3 and 14 μm that the models will be compared with are presented in Sections 4.2 and 5.2. Section 4.4 starts with a description of the LTE radiative transfer disk model to determine the HCN emitting regions. Subsequently, the non-LTE radiative transfer slab model with and without radiative pumping and their results are presented and compared. The results and their conclusions are summarized in Section 5.5.

4.2 HCN emission at 3 and 14 μm

HCN is a linear tri-atomic molecule with three rotational-vibrational modes. These three modes are:

- ν_1 – the C-N stretch at 4.786 μm .
- ν_2 – a doubly degenerate bending at 14.043 μm at $E_u=1025$ K.
- ν_3 – the C-H stretch at 3.019 μm at $E_u=4765$ K.

The two modes that will be further investigated here are the ν_2 and ν_3 modes since they are observable at NIR and MIR wavelengths. The ro-vibrational transitions of the ν_1 mode have very low Einstein A coefficients and have so far not been observed so this mode will therefore not be further investigated. The ν_2 mode is a $\Pi \rightarrow \Sigma^+$ -transition which has a P-,Q- and R-branch following the selection rules. The ν_3 mode is a $\Sigma^+ \rightarrow \Sigma^+$ transition which only allows $\Delta J = \pm 1$, so it has a P- and R-branch but no Q-branch.

4.3 Observations

Observations of the ν_3 mode at 3 μm in emission have been presented by Mandell et al. (2012), where they show detections of HCN for 3 different T Tauri stars, AS 205 N (the northern component), DR Tau and RU Lup. AS 205 N and RU Lup were observed using the spectrometer CRIRES at the Very Large Telescope (VLT) at a spectral resolving power of $R = \lambda / \Delta\lambda = 96,000$, whereas the HCN detection in DR Tau was done with the spectrometer NIRSPEC at the Keck telescope with $R = 25,000$.

The ν_2 mode at about 14 μm was detected in 24 out of 48 T Tauri stars (Salyk et al. 2011) using Spitzer. All three T Tauri stars, AS 205, DR Tau and RU Lup, that show HCN detections at 3 μm also have detections at 14 μm . In this article,

Table 4.1 Parameters used in the specific fiducial disk model for AS 205.

Parameters		Ref. ^a
M_{\star} [M_{\odot}]	1.0	1
R_{\star} [R_{\odot}]	3.7	1
T_{eff} [K]	4250	1
M_{disk} [M_{\odot}]	0.029	1
R_{out} [AU]	200	1
R_i [AU]	0.14	1
h_p/R	0.21	1
α	0.11	1
β	-0.9	1
i [$^{\circ}$]	20	2

^aReferences: (1) Andrews et al. (2009) and (2) Pontoppidan et al. (2011)

AS 205 will be taken as the standard disk for which models of the HCN lines will be made and compared with the observations. Our observations of AS 205 at $3 \mu\text{m}$ (Mandell et al. 2012) show that the P(11) line at $3.0508 \mu\text{m}$ has an absolute flux of $5.6 \cdot 10^{-15} \text{ erg cm}^{-2} \text{ s}^{-1}$ with a calibration uncertainty of about 30%. This can be compared with the total absolute line flux between $13.837 - 14.075 \mu\text{m}$ of $2.2 \cdot 10^{-13} \text{ erg cm}^{-2} \text{ s}^{-1}$ taken from Salyk et al. (2011). The flux ratio F_3/F_{14} between the line fluxes at 3 and $14 \mu\text{m}$ is therefore $2.5 \cdot 10^{-2}$ with an uncertainty of about 40%. It is important to note that AS 205 is a binary and that the P(11) $3 \mu\text{m}$ line observed with CRIRES resolves the binary, with the reported flux consisting of just the emission from AS 205 N. In contrast, the $14 \mu\text{m}$ line flux applies to both sources since Spitzer cannot resolve the binary. The assumption is that the majority of the $14 \mu\text{m}$ line flux comes from AS 205 N. This seems to be a reasonable assumption since the F_3/F_{14} flux ratio is $9.0 \cdot 10^{-2}$ and $1.1 \cdot 10^{-2}$ for RU Lup and DR Tau respectively based on using the R(6) and R(17) lines at $3 \mu\text{m}$ for these sources.

4.4 Radiative transfer models and their results

Three different types of models will be used to simulate the excitation of HCN to investigate which model can best describe the observed line emission. These models are a LTE radiative transfer disk model, a non - LTE radiative transfer slab model and a non-LTE radiative transfer slab model including radiative pumping.

4.4.1 A standard disk model using LTE

As a first step, a LTE disk model is run to investigate how the HCN flux ratios from such a model compare with the observations. In addition this model provides an indication of the regions of the disk from which the 3 and $14 \mu\text{m}$ lines originate and their physical conditions. The continuum radiative transfer disk model called

4 Investigation of HCN excitation in protoplanetary disks

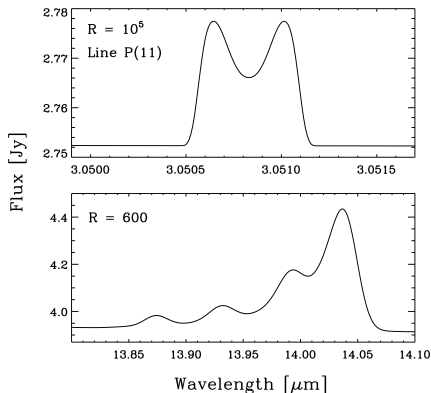


Figure 4.1 Modeled HCN emission using the radiative transfer disk model RADLite for AS 205 N at two different spectral resolving power $R=600$ (*Spitzer*) and 10^5 (CRIRES-VLT). In the upper figure the P(11) line at $3 \mu\text{m}$ is shown and in the lower figure the HCN emission lines between $13.837 - 14.075 \mu\text{m}$.

RADMC (Dullemond & Dominik 2004) was used together with the line raytracing code RADLite (Pontoppidan et al. 2009) to model the $3 \mu\text{m}$ P(11) line and the $14 \mu\text{m}$ line emission between $13.837 - 14.075 \mu\text{m}$, see Fig. 4.1. This model takes into account both radial and vertical temperature and density variations, the motion of the gas, the continuum opacity and the geometry of the disk.

The disk model parameters used in RADMC are those appropriate for the circumstellar disk of AS 205 N. This disk is chosen to be a good model for a typical protoplanetary disk since it has been modeled in detail before and its disk parameters are reasonably well known (Andrews et al. 2009, Pontoppidan et al. 2011). The different parameters are: the mass of the central source (M_\star), its radius (R_\star) and effective temperature (T_{eff}), the mass of the disk (M_{disk}), outer radius of the disk (R_{out}), a flaring parameter $H/R \propto R^\alpha$, an outer pressure scale height (h_p/R), radial surface density $\Sigma = R^\beta$ and an inner radius (R_i) which sets the inner temperature, see Table 1. The initial values for these parameters are taken from previous observational constraints, primarily from sub-millimeter observations (Andrews et al. 2009), and are the same as adopted in (Mandell et al. 2012). Figure 4.2 shows the density and temperature structure of the modeled disk.

The modeling procedure for estimating the line intensities centers around the axisymmetric ray-tracing code called RADLite, the details of which are described extensively in Pontoppidan et al. (2009). RADLite calculates the emission intensity and the spectral line profile for a specific molecular transition by combining the emission from a grid of points across the projected surface of the disk. This allows us to accurately reproduce the effects of the Keplerian rotation of the disk and

4.4 Radiative transfer models and their results

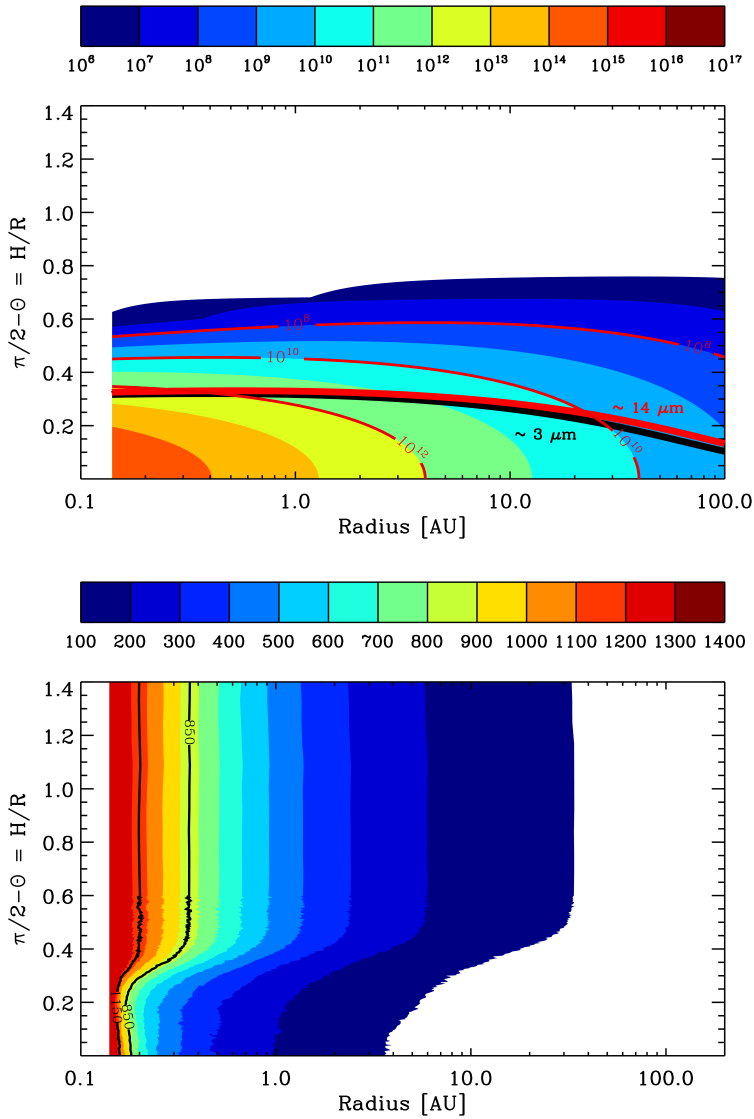


Figure 4.2 Upper panel: Contour plot of the adopted density distribution in the AS 205 N protoplanetary disk. The dark red solid lines mark the densities 10^8 , 10^{10} and 10^{12} cm^{-3} and illustrate the region in the disk where the HCN emission originates. The red and black broader solid lines represent where the dust reaches an optical depth of $\tau = 1$ for $14 \mu\text{m}$ and $3 \mu\text{m}$ lines, respectively. Lower panel: Contour plot of the adopted temperature distribution in the AS 205 N protoplanetary disk. The black solid lines mark the temperature range between 850 – 1150 K and illustrates the region in the disk where most of the HCN emission originates.

Table 4.2 Observations of the R(11) line flux at $3\ \mu\text{m}$ and the $14\ \mu\text{m}$ total line flux between $13.837 - 14.075\ \mu\text{m}$ and their modeled fluxes using a LTE protoplanetary disk model.

	Observations	LTE disk Model ^a
$3\ \mu\text{m}$ P(11) line [$\text{erg cm}^{-2}\ \text{s}^{-1}$]	$5.6 \cdot 10^{-15}$	$3.5 \cdot 10^{-15}$
14 line emission ($13.837 - 14.075\ \mu\text{m}$) [$\text{erg cm}^{-2}\ \text{s}^{-1}$]	$2.2 \cdot 10^{-13}$	$5.1 \cdot 10^{-13}$
3/14 μm flux ratio	$2.5 \cdot 10^{-2}$	$6.8 \cdot 10^{-3}$

^aA relative HCN abundance of $2.0 \cdot 10^{-7}$ to H_2 is used in the models.

the radial surface density and temperature profiles. The initial temperature and density structure of the disk is calculated using the RADMC two-dimensional continuum Monte-Carlo radiative transfer code using standard dust opacities (Dullemond & Dominik 2004), and the dust temperature and source functions for each grid point are generated and then used as input for RADLite. The gas is currently assumed to be coupled with the dust, i.e., the gas temperature is set to be the same as the dust temperature. The gas/dust ratio is set to 12,800 which is based on earlier modeling of water emission lines in T Tauri stars using RADLite (Meijerink et al. 2009) To calculate the emission intensity, the level populations must first be calculated assuming a specific excitation mechanism. The standard formulation assumes local thermodynamic equilibrium (LTE), in which all the level populations are defined by the local temperature at that grid point.

LTE line fluxes and ratio

A relative HCN abundance of $2.0 \cdot 10^{-7}$ to H_2 was used to model the P(11) line at $3\ \mu\text{m}$ and the lines between $13.837 - 14.075\ \mu\text{m}$ since this was the relative abundance that Mandell et al. (2012) found when they fitted the $3\ \mu\text{m}$ lines for AS 205 using LTE excitation. The modeled lines can be seen in Fig. 4.1. The line flux of the P(11) line is about $3.5 \cdot 10^{-15}\ \text{erg cm}^{-2}\ \text{s}^{-1}$ which is close to the observed flux of $5.6 \cdot 10^{-15}\ \text{erg cm}^{-2}\ \text{s}^{-1}$. The modeled lines between $13.837 - 14.075\ \mu\text{m}$ have a total flux of $5.1 \cdot 10^{-13}\ \text{erg cm}^{-2}\ \text{s}^{-1}$ which is about a factor of two higher than the observed total line flux of $2.2 \cdot 10^{-13}\ \text{erg cm}^{-2}\ \text{s}^{-1}$. The 3 / 14 μm flux ratio in this model is inferred to be $6.8 \cdot 10^{-3}$, about a factor of 4 lower than the observed flux ratio of $2.5 \cdot 10^{-2}$, see Table 4.2. Hence either the $3\ \mu\text{m}$ flux is underestimated or the $14\ \mu\text{m}$ flux is overestimated when using the LTE radiative transfer disk model. This may reflect that the disk photosphere, which is the region assumed to be the origin of both the 3 and $14\ \mu\text{m}$ line emission, has a range of densities below the critical densities of these two transitions. Densities below the critical density means that collisions cannot maintain the level populations and, hence, a LTE model will not describe the emission well. In addition, the lines may be radiatively pumped by the stellar or disk radiation field. Radiative pumping will also drive the populations on the different excitation levels away from LTE values.

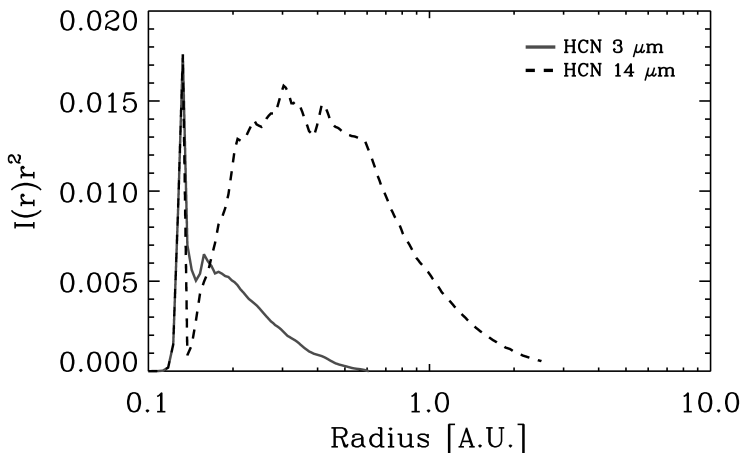


Figure 4.3 The spatial extent of HCN at $3 \mu\text{m}$ and $14 \mu\text{m}$ based on characteristics of AS 205 N LTE model (see Table 4.1). The inclination is set to 45° for illustration purposes.

Spatial extent of 3 versus $14 \mu\text{m}$ emission

The spatial extent of the 3 relative to the $14 \mu\text{m}$ emission is important to investigate since this will help to understand the HCN excitation processes that dominate in different regions of the disk. An estimate of the distribution of the 3 and $14 \mu\text{m}$ emission is therefore made using the raytracing code RADLite, which can, by using the temperature and density structure from RADMC, calculate an intensity image containing an isovelocity curve for a given line and velocity. An isovelocity curve consists of the emission for a specific line at a certain velocity which originates alongside the curve of the disk for which the projected velocity is constant. For more details see Pontoppidan et al. (2009). An image cube consisting of a sample of intensity images within a velocity range of $-100 - +100 \text{ km s}^{-1}$ with a sampling of 0.5 km s^{-1} was made for the $3 \mu\text{m}$ P(11) line and for the $14 \mu\text{m}$ R(17f) line. The disk parameters used are those given in Table 4.1. However, an inclination 45° is used to get a symmetric distribution in the intensity map along the cut through the center of the disk. The intensity map accounts only for emission from the upper surface of the disk which is directed toward the observer since the other side is not seen due to the fact that the disk is optically thick to the continuum photons and hence the view from the other side of the disk is blocked by the dust.

The images in the intensity maps in the image cube were then added and the total intensity along a cut through the disk times R^2 is plotted in Fig. 4.3, where R is the radius of the disk. The intensity times R^2 is chosen since the integrated area of the curve will give the contribution of that region to the flux of the line.

As can be seen in Fig. 4.3 both lines show two peaks. The primary peak close to the star is the emission which comes from the hot inner rim of the disk where it is hit directly by the radiation from the star and the secondary peak represents the emission originating a bit further out in the flared disk where the gas is warm enough to excite and emit the 3 and 14 μm line emission, respectively. More than 50% of the 3 μm line emission originates from within 0.2 AU (for an inner radius of 0.14 AU), whereas about 50% of the 14 μm line emission originates within 0.4 AU. The 14 μm emission is therefore, as expected, excited in a somewhat colder gas region of the disk than the 3 μm emission. Based on these results, we will assume that most of the HCN emission comes from a region in the disk within a temperature range of 850 – 1150 K and volume density range of $10^8 - 10^{12} \text{ cm}^{-3}$ (Fig. 4.2). The density estimate is in addition based on the fact that the dust reaches $\tau = 1$ within that density range for the 3 and 14 μm continuum emission. This is specified in Fig. 4.2 where $\tau = 1$ is emphasized with a black and red line for 3 respectively 14 μm . It is important to note however that the spatial distributions are based on the temperature and density structure estimated by RADMC, which does not separate the gas and dust temperatures in the disk surface, so it will underestimate the contribution from hot material at larger distances.

4.4.2 Non-LTE excitation of HCN using a slab model

The non-LTE radiative transfer slab model RADEX (van der Tak et al. 2007) is used to model both the 3 μm (in the P(11) line) and 14 μm (the integrated intensity between 13.837 – 14.075 μm) line emission fluxes to investigate how the fluxes change with the column density of HCN, the kinetic temperature and the volume density of H_2 . Other input parameters, which we will keep fixed in our analysis, are the width of the molecular line ΔV which is here set to 1 km s^{-1} , the cosmic microwave background radiation which is set to be the same as that from a blackbody with a temperature of 2.73 K and the characteristics of the collisional partners for which we will adopt H_2 . All results scale as $N/\Delta V$. The molecular data for HCN include the statistical weights and energies for all levels and the Einstein A coefficients for all radiative transitions.

For pure rotational transitions within the ground vibrational state, the collisional de-excitation rate coefficients were taken from the Leiden atomic and molecular database (Schöier et al. 2005) based on the data from Dumouchel et al. (2010). Data are only available for temperatures up to 500 K. For temperatures above 500 K, the collisional de-excitation rate coefficients have been set equal to those at 500 K for the different line transitions and the mean velocity dependence on temperature is ignored. To obtain rate coefficients for pure rotational transitions within the excited vibrational states, the $v=0$ values were scaled using the formulation of Chandra & Sharma (2001). For transitions between vibrational states, experimental measurements at 300 K have been made by Smith & Warr (1991, their Table 2). These values apply to the vibrational bands as a whole. Collisional rate

coefficients for individual vibration-rotation transitions have been derived by D. Harsono using a modified version of the formulation of Clary (1983).

The upward collisional rate coefficients (C_{lu}) are determined using Equation 4.1,

$$C_{lu} = \frac{g_u}{g_l} C_{ul} \exp[-E_{ul}/kT], \quad (4.1)$$

where E_{ul} is the energy difference between the two levels and g_u and g_l are the statistical weights for the upper and lower level.

The experimental data of Smith & Warr (1991) show that collisional de-excitation of the ν_2 band at 14 μm by H_2 is much more rapid (by a factor of ~ 300) than that of the ν_3 band at 3 μm . Typical values are $1.5 \sim 10^{-11}$ and $5 \times 10^{-14} \text{ cm}^3\text{s}^{-1}$. Since the Einstein A coefficients of the two bands are 3.3 and 81.7 s^{-1} , respectively, this means that the critical densities A_{ul}/C_{ul} are 2×10^{11} and $1.6 \times 10^{15} \text{ cm}^{-3}$. Thus, the densities needed to excite the 3 μm band are roughly 4 orders of magnitude larger than those for the 14 μm band. Results of the non-LTE calculations are presented below in §4.4.

4.4.3 Non-LTE slab model including radiative pumping

Besides collisions, the HCN lines can also be radiatively pumped. To investigate how this will affect the line fluxes for the 3 and 14 μm emission, an IR radiation field was added in the non-LTE slab model simulated by RADEX. The radiation field is estimated using the RADMC radiative transfer code for the AS 205 disk model using the parameters given in Table 1. Using the resulting dust temperature and density structure, a radiation field in each grid point in the modeled disk is computed. The radiation field in the grid points within the temperature range 850 – 1150 K and volume densities of 10^8 , 10^{10} and 10^{12} cm^{-3} has been extracted. These temperature and density ranges were selected because the LTE analysis in Section 4.4.1 shows them to be typical for the region from where the HCN line emission originates. At wavelengths larger than a few micron the photon noise in this Monte Carlo method is considerable and we have smoothed these results. The radiation field does not change much within the volume density range of 10^8 – 10^{12} cm^{-3} . Hence we have adopted the average radiation field indicated by the red line. The blue line shows a blackbody for 1000 K which is clearly not a good approximation for the averaged radiation field. However, the green line shows a blackbody for 1000 K, scaled with the dilution factor W set to 0.2, which provides a fair fit to the radiation field at wavelengths > 3 micron. In these calculations, we will adopt a blackbody at 1000 K with a dilution factor of 0.02 and 0.2 to estimate the effect of a radiation field on the HCN line emission (see Fig. 4.4).

4 Investigation of HCN excitation in protoplanetary disks

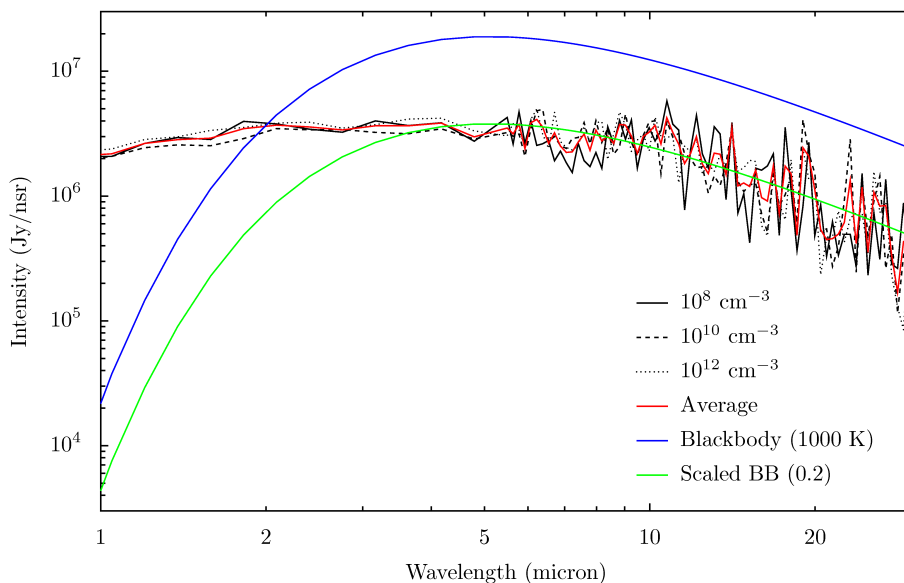


Figure 4.4 The extracted radiation field (in black) using the radiative transfer model RADMC of the standard AS 205 disk for three different volume densities: 10^8 (solid), 10^{10} (dotted) and 10^{12} cm^{-3} (dashed). Their average radiation field is plotted in red. The radiation from a blackbody at 1000 K is plotted in blue and the same blackbody with a dilution factor of 0.2 is presented in green.

4.4.4 Results introducing non-LTE and radiative pumping of HCN

Figure 4.5 shows the 3 and 14 μm line fluxes as a function of the volume density of H_2 for four different temperatures, 300, 600, 900 and 1200 K, and two different HCN column densities 10^{13} (black line) and 10^{15} cm^{-2} (red line). The ratio of the 3 and 14 μm fluxes is shown in the bottom 4 panels shown in Fig. 4.5. In addition, the computed fluxes including the radiation field with a dilution factor of 0.2 (dashed lines) and a radiation field including a dilution factor of 0.02 (dashed dotted lines) are plotted in the figure.

Fig. 4.5 shows, as expected, that the flux (not including a radiation field) increases with both the volume density and the column density. At low density, the line flux increases with $n(\text{H}_2)N(\text{HCN})$ and hence, for constant column density, the line flux scales linearly with density. At high densities ($n \gg n_{cr}$), the line fluxes scale with $N(\text{HCN})$ and becomes independent of $n(\text{H}_2)$. The main difference between the 3 and 14 μm lines is that the 14 μm flux starts to flatten out at around 10^9 cm^{-3} while the 3 μm flux keeps increasing until a much higher density of 10^{14} cm^{-3} . Essentially the 14 μm flux reaches LTE, hence collisional excitation takes over, at a much lower density than the 3 μm flux. This reflects the much higher critical density for the 3 μm line (10^{15} cm^{-3}) than the 14 μm emission lines (10^{11} cm^{-3}). It can clearly be seen in the figure that the 3/14 μm flux ratio is sensitive to density between 10^9 and 10^{14} cm^{-3} , i.e., the density range where the 14 μm levels have reached LTE while the 3 μm flux still increases. However, as expected, no difference in the 3/14 μm flux ratio is apparent between the two different column densities of 10^{13} and 10^{15} cm^{-2} since both types of lines are optically thin.

Another way to plot these results is shown in the left and middle panel of Fig. 4.6 which presents loci in the $n - T$ plane of a constant flux (10^{-8} , 10^{-7} and $10^{-6} \text{ erg cm}^{-2} \text{ s}^{-1}$ for the 3 μm line P(11) and 0.01, 0.05 and 0.1 $\text{erg cm}^{-2} \text{ s}^{-1}$ for the 14 μm flux) for the two different HCN column densities 10^{13} and 10^{15} cm^{-2} . These figures illustrate that when the density is lowered a higher gas temperature is needed to give the same flux of the line and that this effect is stronger for the 3 μm emission than the 14 μm emission. Essentially, the line flux scales with the Planck function at the excitation temperature of the levels. For a two level system, the excitation temperature, T_x is given by

$$\frac{T_x}{T} = \left[1 + \frac{kT}{E_{ul}} \ln \left(1 + \frac{n_{cr}}{n} \right) \right]^{-1} \quad (4.2)$$

Thus for a lower density a higher temperature is needed to collisionally excite the lines to achieve the same intensity in the lines. Only when the density exceeds the critical density will (T_x) approach T and will the line flux become constant. Because E_{ul} is larger for the emission at 3 μm than for the emission at 14 μm , the 14 μm lines need less of a temperature change to compensate for a change in the volume density as the 3 μm emission. The right panel of Fig 4.6 shows the

4 Investigation of HCN excitation in protoplanetary disks

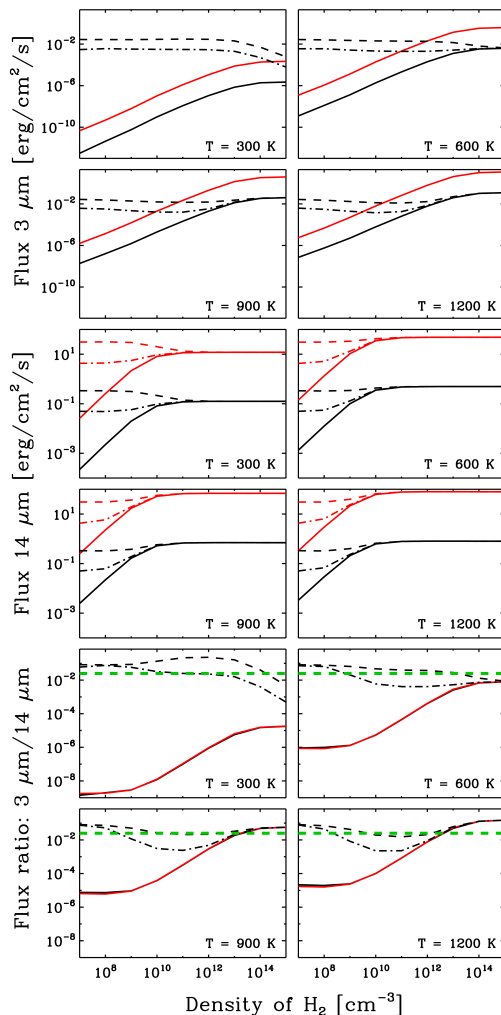


Figure 4.5 The modeled line flux of the HCN P(11) line ($3.0305 \mu\text{m}$), the total HCN line flux between $13.837 - 14.075 \mu\text{m}$ and the $3/14 \mu\text{m}$ line flux ratio as a function of density using a slab model at four different temperatures 300, 600, 900 and 1200 K and for two different column densities. The dashed lines represent a slab model for a HCN column density of 10^{13} cm^{-2} including a radiation field using a blackbody of 1000 K which is scaled with a dilution factor of 0.2 and the dashed-dotted line includes a radiation field using a blackbody for 1000 K which is scaled with a dilution factor of 0.02. The two different HCN column densities (10^{13} and 10^{15} cm^{-2}) are represented by the black and red color on the different types of lines. The observed $3/14 \mu\text{m}$ line flux ratio for AS 205 N is shown in the four lower panels (green dashed line).

4.4 Radiative transfer models and their results

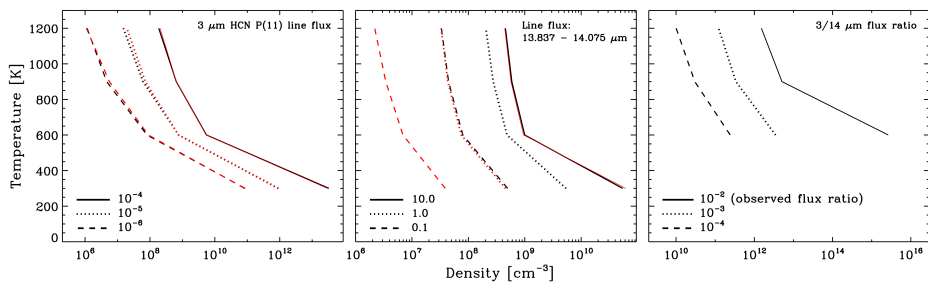


Figure 4.6 Curves of constant P(11) HCN line flux, 13.837 – 14.075 μm total HCN line flux and 3/14 μm HCN flux ratios are plotted as a function of density and temperature for models without radiative excitation. Black (red) lines are for a column density of 10^{13} (10^{15}) cm^{-2} . Left panel: The three different fluxes are 10^{-6} (dashed line), 10^{-5} (dotted line) and 10^{-4} (solid line) $\text{erg cm}^{-2} \text{s}^{-1}$. Middle panel: The three different fluxes are 0.1 (dashed line), 1.0 (dotted line) and 10.0 (solid line) $\text{erg cm}^{-2} \text{s}^{-1}$. Right panel: The three different ratios are 10^{-4} (dashed line), 10^{-3} (dotted line) and 10^{-2} (solid line).

temperature and volume density that are needed to get three different 3/14 μm flux ratios 10^{-2} , 10^{-3} and 10^{-4} . There is no difference in this curve between the different HCN column densities 10^{13} and 10^{15}cm^{-2} .

As can be seen the observed flux ratio of $2.5 \cdot 10^{-2}$ can only be reached with a minimum volume density of $5.0 \cdot 10^{12} \text{cm}^{-3}$ at temperatures $>900 \text{K}$ if no radiative pumping is included. However, at a temperature of 900K , which is also close to what is estimated for three different T Tauri stars using a LTE slab model for HCN (Mandell et al. 2012), the emission would originate in a region with a volume density of around $10^{13} - 10^{14} \text{cm}^{-3}$ according to Fig. 4.5. These high densities are only reached below the limit where the 3 and 14 μm continuum emission becomes optically thick. Based on Fig. 4.2, the HCN emission is expected to arise in a region with densities of $10^8 - 10^{12} \text{cm}^{-3}$. Hence, including non-LTE without radiative pumping cannot re-produce the observed flux ratio. Therefore an infrared radiation field is included in the non-LTE slab model to see if this may be able to explain the observed flux ratio.

Including the radiation field leads to higher line fluxes. The radiation field will dominate over collisions when

$$\frac{n_{crit}}{n} \frac{W}{\exp[h\nu/kT_R] - 1} \gg 1 \quad (4.3)$$

where T_R is the temperature of the radiation field (1000K in our case). This happens when the volume density is much lower than the critical density or when $h\nu/kT_R \ll 1$. When the radiation field dominates, the line fluxes scale with the dilution factor times the Planck function at the excitation (=radiation) temper-

ature. As a result, at low densities and temperatures, the calculated line flux is much higher than expected from a pure collisional model (Fig. 4.5). At densities above the critical density, the ‘collisional’ results are recovered. Again, the effects are larger at shorter than at longer wavelengths because of the higher critical densities for the $3\ \mu\text{m}$ lines. This explains why the flux ratio is higher at the lower volume densities and temperatures, since this is the region where the radiation field dominates over the collisions and the excitation temperature is close to the radiation temperature.

The green line in Fig. 4.5 indicates the observed $3/14\ \mu\text{m}$ flux ratio. It is seen that the models including radiative pumping at a dilution factor of 0.2 now reproduce the observed flux ratio (within a factor of a few) over a very wide range of densities and temperatures, including the range of densities of $10^8 - 10^{12}\ \text{cm}^{-3}$ appropriate for the upper disk layers from which the HCN emission is thought to originate. For the smaller dilution factor of 0.02, the flux ratio drops somewhat below the observed value in the relevant density range, but still provides a closer match to the observational data than the model without a radiation field. That the flux ratio is getting closer to the observed flux ratio over a wide range of densities when including an infrared radiation field demonstrates that infrared radiative pumping may play an important role when exciting the HCN molecules in the inner region of a protoplanetary disk atmosphere.

Note that the flux ratio is not sensitive to the HCN column density: only the absolute fluxes can give estimates of the HCN column density and thus its abundance.

4.5 Summary and conclusions

The excitation processes leading to the observed HCN emission from circumstellar disks around T Tauri stars have been studied to investigate which type of slab or disk model can best describe the observations that have been made so far. This work shows that the $3\ \mu\text{m}$ HCN emission is not well described with a LTE slab or disk model and that these type of models will overestimate the flux of the lines, hence underestimate the abundance of HCN. As an example, judging from Fig. 4.5, assuming LTE, the line fluxes are overestimated by about an order of a magnitude at a temperature of 900 K and a volume density of $10^{12}\ \text{cm}^{-3}$ if no radiative pumping is included. Hence, the derived column density (eg., the HCN abundance) would be underestimated by about an order of magnitude. For lower densities, the effect would be proportionally larger. This is because the critical density for the $3\ \mu\text{m}$ emission is much higher than the density of the inner (<0.2 AU) regions of the upper parts of the disks from which the emission is thought to arise. LTE is a better approximation for the $14\ \mu\text{m}$ HCN emission due to its lower critical density. Non-LTE models are better at describing the observed $3\ \mu\text{m}$ emission if infrared radiative pumping is included in the models.

These results can be compared to the work done on H_2O emission originating

from the same region in protoplanetary disks by Meijerink et al. (2009). They show that also water emission coming from <0.2 AU is not well modeled using LTE slab or disk models. The water emission lines are also better described when including non-LTE excitation in their disk model. They in addition show that the higher vibrational band lines are even more sensitive to non-LTE effects. Mandell et al. (2012) illustrate that the line fluxes of the higher ro-vibrational band $\nu = 2-1$ of HCN is overestimated in their LTE disk model compared with the observed upper limits. This can be explained by the fact that the higher ro-vibrational line fluxes, as for HCN nu_3 and the H₂O lines, are lowered when introducing non-LTE in the models. Future work investigating the impact on the higher ro-vibrational lines when including non-LTE and radiative pumping in a full disk model would therefore be interesting.

Acknowledgements

The authors are grateful to Kees Dullemond for providing the RADMC code and Klaus Pontoppidan for making his RADLite code available. JEB is supported by grant 614.000.605 from Netherlands Organization of Scientific Research (NWO). EvD acknowledges support from a NWO Spinoza Grant and from Netherlands Research School for Astronomy (NOVA).

